Investigation on optical and photoluminescence properties of organic semiconductor Al-Alq_3 thin films for organic light-emitting diodes application

Fan Zhang (张 帆), Cong Wang (王 聪), Kai Yin (银 恺), Xinran Dong (董欣然), Yuxin Song (宋雨欣), Yaxiang Tian (田亚湘), and Ji'an Duan (段吉安)*

State Key Laboratory of High Performance and Complex Manufacturing, College of Mechanical and Electrical Engineering, Central South University, Changsha 410083, China

**Corresponding author: duanjian@csu.edu.cn*

Received June 18, 2017; accepted September 22, 2017; posted online October 19, 2017

The optical constants, photoluminescence properties, and resistivity of Al-Alq_3 thin films prepared by the thermal co-evaporation method on a silicon substrate are studied with various Al fractions. A variable angle spectroscopic ellipsometry is employed to determine the optical constants in the wavelength from 300 to 1200 nm at incidence angles of 65°, 70°, and 75°, respectively. Both the refractive indices and extinction coefficient apparently increase with increasing Al fractions. The intensity of photoluminescence spectra gradually increases with decreasing Al fractions due to intrinsic energy level transition of Alq_3 organic semiconductor in the ultraviolet wave band. The resistivity decreases from 42.1 to 3.36 $\Omega \cdot$ cm with increasing Al fraction from 40% to 70%, resulting in a larger emission intensity in photoluminescence spectra for the 40% Al fraction sample.

OCIS codes: 160.4890, 120.2130, 250.5230.
doi: 10.3788/COL201715.111602.

Recently, organic semiconductors have attracted a lot of interest for the application of optoelectronics devices, particularly, organic light-emitting diodes (OLEDs), which is a promising candidate for the next-generation light source to shed clear light on flat panel displays, transparent lighting panels, and luminescent wallpapers due to their high luminescence efficiency, low power consumption, wide spectrum capability, high color contrast, and potentially large area flexible color displays[1–4]. The tri-(8-hydroxy-quinoline) aluminum (Alq_3)[5–7] organic semiconductor as the electron transport and emission material is widely used in efficient multi-layered OLEDs on account of its high fluorescence efficiency, eminent thermal stability, and good electron mobility[8–11]. To intensively comprehend and design of such devices[12], investigation of the optical and photoluminescence (PL) properties of Alq_3 thin films is indispensable, since the efficiency, brightness, and stability of OLED devices are directly determined by the optical properties of the Alq_3 material[13]. In addition, owing to the lifetime and efficiency of the blue OLEDs falling behind those of the green OLEDs[14–16], much endeavor has been dedicated to transform the emission of Alq_3 from the green to the blue region. So far, only a few researches have been reported for metal-doped organic semiconductor films in OLEDs[17,18]. Shi *et al.* have prepared a novel blue-emissive Alq_3 through the pull–push effect[19]. Khan *et al.* have deposited Ag incorporated Alq_3 and found that the PL intensity is enhanced with the Ag concentration[20]. Cuba *et al.* have improved luminescence intensity and stability of Alq_3 films by incorporating 30 wt% of ZnO[21]. Thus, it is intriguing to explore the properties of Al-doped organic semiconductor Alq_3 thin films for OLED applications.

In this Letter, the optical, PL, and resistivity properties of Al-Alq_3 thin films with different Al fractions have been studied in detail.

The Al-Alq_3 thin film was deposited by the co-evaporation technique on *n*-type Si (111) 2–4 $\Omega \cdot$ cm resistivity substrate overlaying a native SiO_2 layer. Before deposition, distilled deionized water and ethanol were used for cleaning Si substrates. Al-Alq_3 thin films with different Al volume fractions can be acquired by accurately controlling the evaporation rates of Al and Alq_3 under base chamber pressure of 1×10^{-4} Pa. A quartz crystal thickness monitor (Sigma SQM-160) can acquire the film thickness and the evaporation rate. The resistance of Al-Alq_3 was measured using a Keithley 2400 sourcemeter. The film surface morphology was characterized by an atomic force microscope (AFM, Bruker Dimension Icon VT-1000 System) in the tapping mode. The PL intensity was measured at room temperature by exciting the samples at normal incidence with a He-Cd laser (325 nm). PL spectra have been acquired by collecting the emitted luminescence at a normal direction with a 0.5 m spectrometer (Acton Research, Spectra Pro 500i). The optical properties of the sample have been measured using a spectroscopic ellipsometer (Sopra GES5E) with a wavelength from 300 to 1200 nm at three different incident angles of 65°, 70°, and 75°, respectively.

The AFM results in Fig. 1(a) exhibit a crack-free and smooth surface with a 1.57 nm surface roughness, which is beneficial for spectroscopic ellipsometry (SE) measurement, since intense scattering from a rough surface can lead to optical depolarization. SE measurements yield a complex reflectance ratio[22,23],

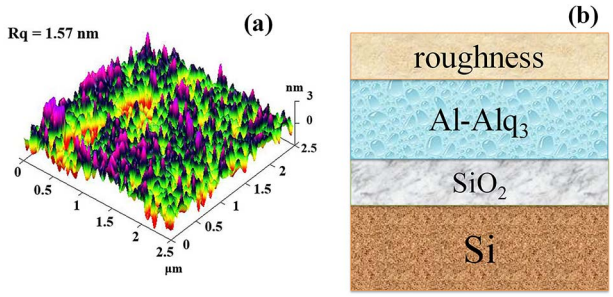

Fig. 1. (a) AFM image of the Al-Alq_3 sample; (b) schematic diagram of the four-layer structure model applied in the SE data fitting.

$$\rho = r_p/r_s = \tan\psi \exp(\Delta), \tag{1}$$

where r_p and r_s are the Fresnel reflection coefficients of parallel (p) and perpendicular (s) polarized light, respectively. Further, ψ and Δ are the amplitude ratio of reflected p- to s-polarized light and the phase shift difference, respectively. With the purpose of obtaining the complex refractive index $N(E) = n(E) + ik(E)$ of the Al-Alq_3 sample, the ψ and Δ derived from the SE measurement can be fitted to an appropriate optical model and dispersion model. A four-layered optical model (surface roughness layer/Al-Alq_3 layer/SiO_2 layer/Si substrate), as shown in Fig. 1(b), has been employed in the SE fitting procedure, where the surface roughness layer is modeled on a Bruggeman effective medium approximation (EMA) theory with a mixture of 50% Al-Alq_3 and 50% voids[24]. The thickness of as-prepared Al-Alq_3 thin films is limited below 150 nm, because thickness values in the range 50–150 nm are typically used in OLED devices. Besides, the thickness of the SiO_2 layer is 1 nm. The optical constant of which is referred to in Ref. [25]. The Lorentz oscillation model has been adopted to characterize the optical function of the sample described as follows[26]:

$$\varepsilon_1(\omega) = \varepsilon_{1\infty} + \sum_{j=1}^{m} \frac{F_j(\omega_j^2 - \omega^2)}{(\omega_j^2 - \omega^2)^2 + (\omega\Gamma_j)^2}, \tag{2}$$

$$\varepsilon_2(\omega) = \sum_{j=1}^{m} \frac{F_j\omega\Gamma_j}{(\omega_j^2 - \omega^2)^2 + (\omega\Gamma_j)^2}, \tag{3}$$

where $\varepsilon_{1\infty}$ is the light-frequency dielectric constant, and m is the total number of oscillators with frequency ω_j, broadening Γ_j, and oscillator strength $F_j = f_j\omega_j^2$, representing the percentage contribution of oscillator j to the whole system. Four oscillators have been chosen, because the spectra can be reproduced with this number of main peaks in the initial point-by-point fit. The data fitting process is then applied by regulating the film thickness and model parameters. The fitting of the Al-Alq_3 thin film at various Al fractions exhibits an excellent agreement with experimental data in the whole measured spectral range, as shown in Fig. 2, which declares that the fitted dispersion model and optical model are feasible and reasonable.

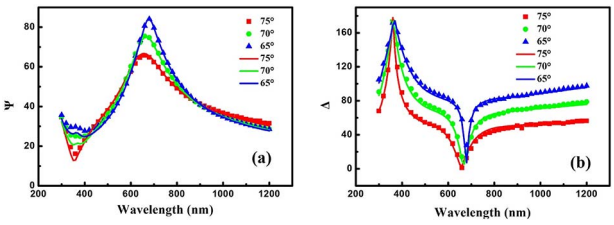

Fig. 2. (Color online) Experimental (dotted lines) and calculated (solid lines) SE data for 40% Al fraction Al-Alq_3 thin film at incidence angles 65°, 70°, and 75°.

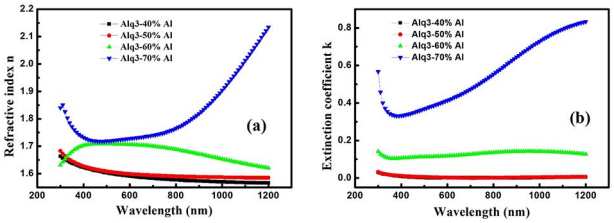

Fig. 3. (Color online) (a) Refractive index n and (b) extinction coefficient k of Al-Alq_3 thin films with various Al fractions.

Figure 3 presents the refractive index n and extinction coefficient k for the series of Al-Alq_3 samples. The refractive index n in Fig. 3(a) apparently increases in the wavelength region from 300 to 1200 nm with the Al fraction increasing from 40% to 70% on account of heavy light refraction in Al rather than those of Alq_3. The density of metal Al is larger than organic Alq_3. Therefore, the compact Al-Alq_3 thin film with 70% fraction will increase the refractive index[27]. The abnormal dispersion turns up in the ultraviolet (UV) band (300–400 nm) for the 60% Al sample and near the infrared band (700–1200 nm) for the 70% Al sample due to strong absorption in this band for the samples[28]. The absorption range of Al-Alq_3 thin films emerges in two wavelength ranges: UV band and near infrared band, as shown in Fig. 3(b), which represents Alq_3 intrinsic absorption and impurity absorption induced by Al, respectively. The extinction coefficient k obviously increases with the Al fraction increasing in the wavelength from 300 to 1200 nm. The onset of absorption defined by the minimum energy value, where k differs from zero appears in the wavelength of 380 nm (=3.26 eV) in the UV absorption band. This is on behalf of the lower limit of the optical gap for Alq_3 organic semiconductor and is in accordance with previously reported values of 2.65[29] and 2.64 eV[30]. On the other hand, the impurity absorption peak in the near infrared band is derived from the impurity energy level induced by the Al in sample. Hence, the k values in the wavelength after 800 nm exhibit increases, particularly in the 70% Al sample.

Figure 4(a) has displayed the PL spectra of various Al fraction in the Al-Alq_3 sample. The intensity of the PL spectra gradually increases with the Al fraction decreasing from 70% to 40%. It signifies that impure Al restrains the

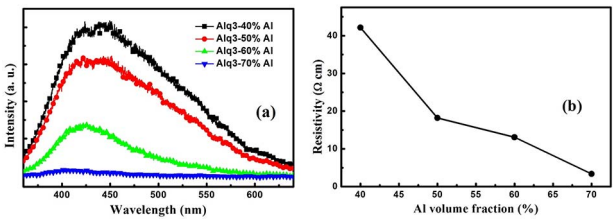

Fig. 4. (Color online) (a) PL spectra of Al-Alq_3 thin films with different Al fractions. (b) The resistivity as a function of the Al volume fraction in Al-Alq_3 thin films.

luminescence of Al-Alq_3 thin films, since the luminescence is attributed to intrinsic energy level transition of Alq_3 organic semiconductor in the UV band rather than those of metal Al in the near infrared band. A He–Cd laser (325 nm) can easily excite PL emission of around 420 nm (blue–violet) in the intrinsic absorption zone. The emission is related to the recombination of free excitons in an exciton–exciton collision process on the near band-edge transitions[31]. Further, the PL emission shifts from the wavelength of 439 to 408 nm with the Al fraction enlarging from 40% to 70%. The blue shift phenomenon is dominated by defect-related deep-level emission from the Al impurity for the OLEDs application. Figure 4(b) shows the resistivity of Al-Alq_3 thin films with various Al fractions. The resistivity value of samples decreases rapidly from 42.1 to 3.36 $\Omega \cdot$ cm with increasing Al fractions from 40% to 70%. The electrical properties of Al-Alq_3 thin films are correlated to the oxygen content of the sample. The more oxygen deficient generally expresses a lower resistivity[32]. The Al mixing into Alq_3 in Al-Alq_3 thin film leads to charge donation and an increase in conductance[33]. In Al-Alq_3 thin film with high Al fraction, the interconnection of adjacent Al granules develops a continuous conductive network, emerging metal conductive behaviors in specimen. When the excitation light in PL measurement propagates to the surface of Al-Alq_3 thin film, the separated holes will readily spread from the irradiated region to the non-irradiated region, resulting in emission light tremendously dropping off from separated holes. With Al fraction decreasing, the Alq_3 matrix can gradually cut off the connection of Al granules. The Al-Alq_3 slowly exhibits weak conductive behaviors by reason of the high resistivity of Alq_3, leading to larger emission intensity in the PL spectra.

In conclusion, Al-Alq_3 thin films on Si substrates with various Al volume fractions are prepared by a thermal co-evaporation technique. The optical functions (n and k) are acquired by SE in the wavelength region from 300 to 1200 nm at three incidence angles: 65°, 70°, and 75°. The measured SE spectra are fitted by combining a four-layer optical model with EMA and a Lorentz oscillation dispersion model. The refractive indices in the measured wavelength region evidently increase with increasing Al fractions. It emerges to an abnormal dispersion region in the UV band for the 60% Al sample and the near infrared band for the 70% Al sample by reason of strong absorption in this band. The extinction coefficient k apparently increases with the Al fraction increasing in the measured wavelength range, where the onset of absorption is found to be at wavelength of 380 nm. The intensity of PL spectra gradually increases with decreasing Al fractions, since the luminescence is attributed to intrinsic energy level transition of Alq_3 organic semiconductor in the UV band rather than those of metal Al in the near infrared band. Further, the blue shift of the PL emission peak with increasing Al fractions is due to defect-related deep-level emission from an Al impurity. The resistivity value of samples decreases rapidly from 42.1 to 3.36 $\Omega \cdot$ cm with increasing Al fraction from 40% to 70%, resulting in a larger emission intensity in the PL spectra for the 40% sample. This study can shed light on the design and fabrication of Alq_3-based luminescent devices in an OLEDs application.

This work was supported by the National Natural Science Foundation of China (NSFC) (Nos. 91323301 and 51505505), the Natural Science Foundation of Hunan Province (No. 2016JJ3147), the China Postdoctoral Science Foundation (Nos. 2015M572264 and 2016T90757), the Self-selected Topic Fund of State Key Laboratory of High Performance and Complex Manufacturing (No. ZZYJKT2015-08), and the Fundamental Research Funds for the Central Universities of Central South University.

References

1. H. Sasabe and J. Kido, J. Mater. Chem. C **1**, 1699 (2013).
2. B. Geffroy, P. L. Roy, and C. Prat, Polym. Int. **55**, 572 (2006).
3. J. W. Park, D. C. Shin, and S. H. Park, Semicond. Sci. Technol. **26**, 034002 (2011).
4. J. T. Smith, B. O'Brien, Y. K. Lee, E. J. Bawolek, and J. B. Christen, J. Disp. Technol. **10**, 514 (2014).
5. C. Wang, J. Shao, Z. Mu, W. Liu, and G. Ni, Chin. Opt. Lett. **12**, 040402 (2014).
6. W. M. Liu, Y. Zhang, and G. Ni, Opt. Express **20**, 6225 (2012).
7. J. Shao, X. Yuan, Z. Mu, and G. Ni, Chin. Opt. Lett. **14**, 062501 (2016).
8. K. Mullen and U. Scherf, *Organic Light Emitting Devices: Synthesis Properties and Applications* (Wiley VCH, 2006).
9. H. J. Kim, T. Tamura, Y. Nakayama, Y. Noguchi, and H. Ishii, J. Photopolym. Sci. Tech. **25**, 183 (2012).
10. S. Kim, P. Choi, S. Kim, H. Park, D. Baek, S. Kim, and B. Choi, J. Nanosci. Nanotechno. **16**, 4742 (2016).
11. T. Fuhrmann and J. Salbeck, MRS Bull. **28**, 354 (2003).
12. B. Masenelli, A. Gagnaire, L. Berthelot, J. Tardy, and J. Joseph, J. Appl. Phys. **85**, 3032 (1999).
13. I. I. Mikhailov, S. A. Tarasov, I. A. Lamkin, P. O. Tadtaev, L. I. Kozlovich, A. V. Solomonov, and E. M. Stepanov, J. Phys. Conf. Ser. **741**, 012103 (2016).
14. C. Xiang, W. Koo, F. So, H. Sasabe, and J. Kido, Light: Sci. Appl. **2**, e74 (2013).
15. N. H. Kim, Y. H. Kim, J. A. Yoon, S. Yoo, K. W. Cheah, F. Zhu, and W. Y. Kim, Chin. Opt. Lett. **14**, 043001 (2016).
16. G. Shi, J. Wang, C. Xu, X. Li, and Z. Wang, Chin. Opt. Lett. **13**, 042301 (2015).
17. B. Lussem, M. Riede, and K. Leo, Phys. Status Solid. A **210**, 9 (2013).

18. Y. Watanabe, H. Sasabe, D. Yokoyama, T. Beppu, H. Katagiri, Y. J. Pu, and J. Kido, Adv. Opt. Mater. **3**, 769 (2015).
19. M. M. Shi, J. J. Lin, Y. W. Shi, M. Ouyang, M. Wang, and H. Z. Chen, Mater. Chem. Phys. **115**, 841 (2009).
20. M. B. Khan and Z. H. Khan, J. Lumin. **188**, 418 (2017).
21. M. Cuba and G. Muralidharan, J. Fluoresc. **25**, 1629 (2015).
22. H. Tompkins and E. A. Irene, *Handbook of Ellipsometry* (William Andrew, 2005).
23. Y. Meng, S. Chen, and G. Jin, Chin. Opt. Lett. **8**, 114 (2010).
24. B. Fodor, P. Kozma, S. Burger, M. Fried, and P. Petrik, Thin Solid Films **617**, 20 (2016).
25. E. D. Palik, *Handbook of Optical Constants of Solids* (Academic, 1998).
26. A. B. Djurisic, C. Y. Kwong, W. L. Guo, T. W. Lau, E. H. Li, H. S. Kwok, L. S. M. Lam, and W. K. Chan, Thin Solid Films **416**, 233 (2002).
27. H. Kim, A. Pique, J. S. Horwitz, H. Murata, Z. H. Kafafi, C. M. Gilmore, and D. B. Chrisey, Thin solid films **377**, 798 (2000).
28. H. Okuda, K. Takeshita, S. Ochiai, Y. Kitajima, S. Sakurai, and H. Ogawa, J. Appl. Crystallogr. **45**, 119 (2012).
29. C. Himcinschi, N. Meyer, S. Hartmann, M. Gersdorff, M. Friedrich, H. H. Johannes, W. Kowalsky, M. Schwambera, G. Strauch, M. Heuken, and D. R. T. Zahn, Appl. Phys. A **80**, 551 (2005).
30. A. Farahzadia, M. Beigmohamadi, P. Niyamakom, S. Kremers, N. Meyer, M. Heuken, and M. Wuttig, Appl. Surf. Sci. **256**, 6612 (2010).
31. J. Y. Tsutsumi, H. Matsuzaki, N. Kanai, T. Yamada, and T. Hasegawa, JPN J. Appl. Phys. **53**, 05HB12 (2014).
32. F. L. Wong, M. K. Fung, S. W. Tong, C. S. Lee, and S. T. Lee, Thin Solid Films **466**, 225 (2004).
33. S. H. Jeong, S. Kho, D. Jung, S. B. Lee, and J. H. Boo, Surf. Coat. Tech. **174**, 187 (2003).